

DESIGN AND COMMISSIONING OF THE ASU CXLS RF SYSTEM *

B. J. Cook[†], S. P. Jachim, G. I. Babic, J. R. S. Falconer, R. E. Larsen, M. R. Holl, W. S. Graves
Arizona State University, Tempe, AZ, USA

Abstract

The Compact X-ray Light Source (CXLS) uses inverse Compton scattering of a high intensity laser off a bright, relativistic electron beam to produce hard x-rays. The accelerator consists of a photoinjector and three standing wave linac sections, which are powered by two 6 MW klystrons operating at 9.3 GHz with a repetition rate of 1 kHz. This paper presents the design and commissioning of the CXLS RF systems consisting of both high-power RF structures and low power diagnostics. The high-power RF system is comprised of two solid state amplifier and klystron modulator sets, various directional couplers and three phase shifter power dividers. The low-level system consists of a master oscillator and laser phase lock, I/Q modulators, I/Q demodulators, and downconverters. We present measurements of the low-level and high-power RF phase and amplitude stability showing RMS timing jitter in the tens of femtoseconds and amplitude jitter below 0.1% at high power.

INTRODUCTION

Currently as tested the CXLS produces an electron beam capable of exceeding 30 MeV on a beam line that is approximately 10 meters in length. This would not have been possible without significant engineering effort and forethought for the RF system, both in high power delivery and in low power diagnostics. The high power RF energy provided by the two 6 MW klystron modulators, MOD1 and MOD2, are split such that MOD1 is dedicated to the photoinjector and a single linac, whereas MOD2 provides power to the other two linac structures.

DESIGN REQUIREMENTS

Design goals for the RF system were to have less than 1° phase jitter relative to the master oscillator at 9.3 GHz for the laser oscillator and in any accelerator structure. Additionally, both laser pulse arrival timing jitter at the cathode and electron beam timing jitter at the interaction point should be less than 500 fs.

SYSTEM DESCRIPTION

As seen in Fig. 1, the main RF signal for the entire system is 9.3 GHz provided from a master oscillator (MO). The MO is synchronized to a timing signal provided by a GPS module which also drives the timing of the laser and both klystron modulators. The MO also provides various other harmonics, namely 6975 MHz and 2325 MHz signals, used in the low level RF system. Each of these signals were based on their interactions to adjacent frequencies when

attempting to resolve intermodulation products [1]. The 6975 MHz signal acts as a local oscillator (LO) input into the down conversion (DNC) chassis, mixing with an RF input of 9.3 GHz creating a directly proportional 2325 MHz signal. The 2325 MHz is then fed into our In Phase and Quadrature Demodulation (IQD) chassis which provides an I and Q output in both polarities. Amplitude and phase changes are accomplished by adjusting the I and Q inputs to the In Phase and Quadrature Modulation (IQM) chassis or using the 4 port Phase Shifter Power Dividers (PSPD).

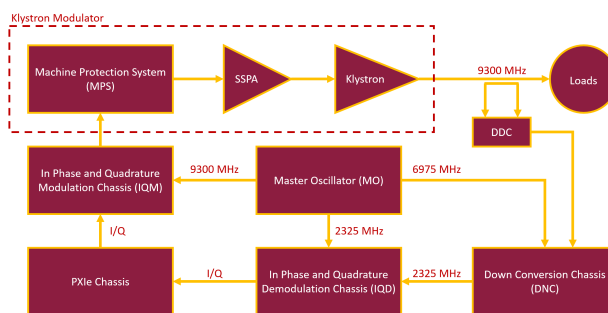


Figure 1: RF system block diagram.

MEASUREMENTS

The 9300 MHz signal output from the klystron modulators is directly measured using a Dual Directional Coupler (DDC) and attenuated to not exceed the input RF limits of the DNC chassis. Whereas the IF output signal is amplified to ensure readability when the signal reaches the PXIe chassis. The driving reason for this is based on measured conversion losses and LO leakage as shown in Figs. 2 and 3. There are notable outliers from this data, specifically with regards to LO Leakage. Those specific devices were placed in spare channels to minimize their impact.

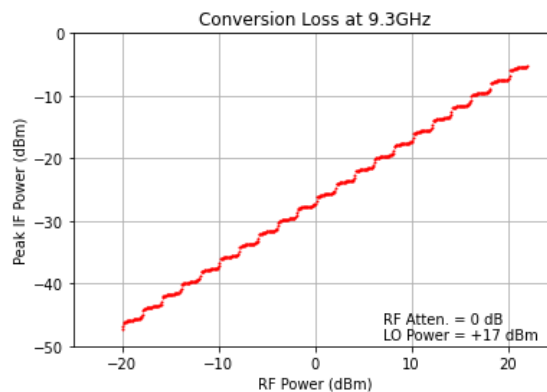


Figure 2: Down converter conversion loss.

* This work is supported in part by NSF award #1935994.

[†] bjcook8@asu.edu

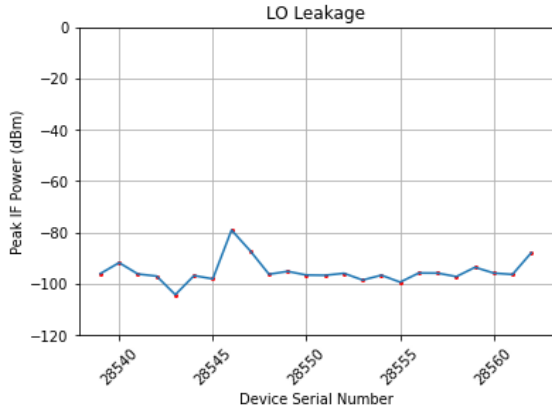


Figure 3: Down converter LO leakage.

Outliers aside, the bulk of the data shows similar losses through the system using the designed maximum inputs to the chassis at +17 dBm RF and +16 dBm LO. The insertion loss through the cables post down conversion provided an approximate output of 200 μ V from the PXIe, barely in the readable range. To compensate for the losses an additional +20 dB amplifier was added to each of the direct outputs from the DNC chassis boosting the signal into the 200 mV range.

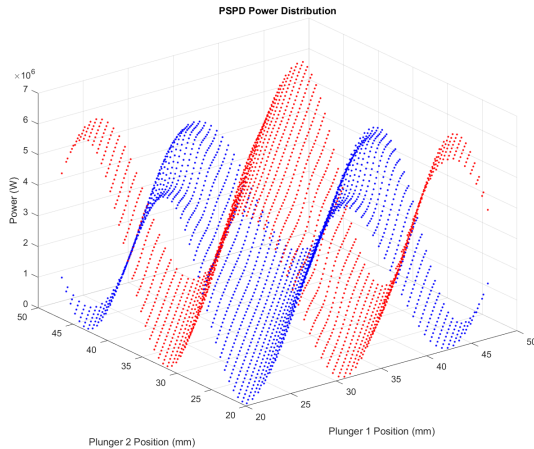


Figure 4: PSPD power split, S_{21} vs. S_{31} .

Prior to providing the high power RF to its loads, understanding the power distribution and phase change through the PSPD was vital. Each of the PSPD's have two motors that adjust plungers to modify the power output ratio and phase. The difference in the motors determine the power distribution whereas the overall height adjusts the phase. Using a Vector Network Analyzer to perform four port S parameter measurements, each of the three PSPD's were profiled using an operational range of 20 mm to 46 mm for each of the motors. A total of 42 measurements were taken in increments of 0.577 mm of adjustment with each providing a full 4x4 S parameter matrix. Post processing the results allowed for the creation of Figure 4 showing the power distribution for S_{21}

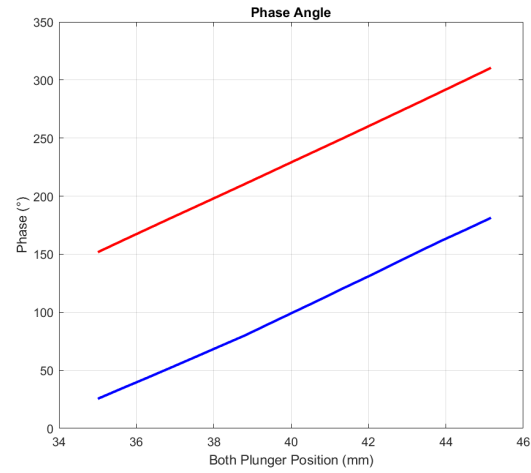


Figure 5: PSPD phase, S_{21} & S_{31} .

and S_{31} in addition to Fig. 5, showing the phase adjustments for the same ports.

Where bulk changes to power and phase are accomplished through adjusting the PSPD's, discrete changes are performed by modifications of the RF drive signal's in-phase (I) and quadrature (Q) components. As seen in reference [2], if the main RF drive signal is defined as,

$$\tilde{g}(t) = g_c(t) + jg_s(t) \quad (1)$$

where $g_c(t)$ and $g_s(t)$ are real-values and therefore can write,

$$g(t) = g_c(t)\cos(2\pi f_c t) - g_s(t)\sin(2\pi f_c t) \quad (2)$$

This allows for the establishment of definitions of I as $g_c(t)$ and Q as $g_s(t)$ all of which with respect to a carrier of $\cos(2\pi f_c t)$. Therefore,

$$a(t) = \sqrt{g_s(t)^2 + g_c(t)^2} \quad (3)$$

$$\phi(t) = \arctan\left(\frac{g_s(t)}{g_c(t)}\right) \quad (4)$$

The above equations facilitates the creation of a time-varying phasor at the origin of a $g_c g_s$ -plane [2]. The phasor is ideally centered on the axis and perfectly symmetrical in rotation as illustrated in Fig. 6a. However, each of the channels required a unique set of calibration factor to compensate for both additive and multiplicative errors within the system as

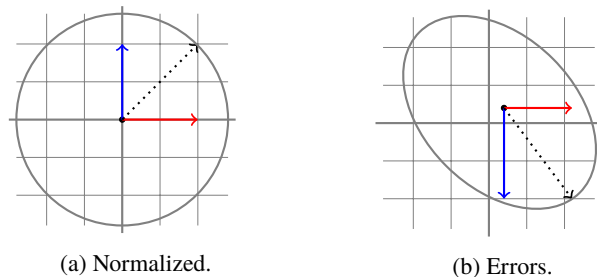


Figure 6: $g_c g_s$ -plane.

illustrated in Fig. 6b. The multiplicative errors stem from both the gain imbalance and quadrature errors, whereas the additive error is reference to the I/Q origin offset within the system.

To determine each channels calibration factor, F_{CAL} , the peak voltage of the Q^+ signal for each channel was measured. By minimizing the I^+ signal, assuming it's effectively zero for calculations, allowed for the initial calculation of the compensation factor (k'), using Eq. (5) and known values of 50Ω matched impedance and supply power. The coupling factor, F_{COUP} , in this case represents the combination of known static attenuation's either inherent in the device or added on to protect the system. Therefore, using Eq. (6) we can calculate F_{CAL} from the known quantity of F_{COUP} and the calculated value for k' .

$$P_S = \frac{k' V_{PK}^2}{2Z_o} \rightarrow k' = \frac{2Z_o P_S}{V_{PK}^2} \quad (5)$$

$$F_{CAL} = k' F_{COUP} \quad (6)$$

The transmission line power, P_{TL} , can then calculated using the following equation,

$$P_{TL} = F_{CAL} \left(\frac{a(t)^2}{2Z_o} \right) \quad (7)$$

Substituting Eq. (3) into Eq. (7), allows for a calibration corrected P_{TL} with respected to the I^+ and Q^+ values.

$$P_{TL} = F_{CAL} \left(\frac{g_s(t)^2 + g_c(t)^2}{100} \right) \quad (8)$$

Each of the 8 channel IQD chassis were corrected using the above strategy by applying a corrective matrix using the P_{TL} values calculated in Eq. (8). Validation of the corrections were able to produce similar graphs to what is displayed in Fig. 6a. However, some channels required further tweaking due to slight deviations in the insertion loss measurement, F_{COUP} . This was initially seen as slight deviations in power during 360° phase adjustments of the IQM.

Using the calibrated system, both low and high power jitter measurements were performed on the system. Initially the lower power settings were used to establish the results documented in Table 1. The power jitter at this level, as seen in the first column, is very close and well within the design parameters of the system. The phase jitter as measured is 0.16° for both klystrons which corresponds to a distance of $14.34 \mu\text{m}$ or 47.79fs . The same data is post processed to factor out drift inherit in the system and is showcased in the "Short Jitter" column. The adjusted values drop down to

Table 1: Low Power Jitter Measurements

Device	Power Jitter	Phase Jitter	Short Jitter
MOD1	0.42 %	0.161°	0.094°
MOD2	0.49 %	0.169°	0.139°

0.094° and 0.139° phase jitter for MOD1 and MOD2, which presents a more accurate assessment of the phase jitter in the system. The same methodology was done at higher powers as shown in Table 2. Once again, the power jitter for both klystron modulators was well within the design parameters. The jitter, albeit very low, is significantly different between MOD1 and MOD2. MOD2 is seeing 0.076° which corresponds to $6.81 \mu\text{m}$ or 22.7fs . Whereas MOD1 is at 0.212° corresponding to $18.98 \mu\text{m}$ or 62.72fs , effectively triple the value of MOD2. Even though the jitter in both devices is low, additional investigations into both the low level RF noise and individual modulator performance are on-going.

Table 2: High Power Jitter Measurements

Device	Power Jitter	Phase Jitter	Short Jitter
MOD1	0.19 %	0.418°	0.212°
MOD2	0.15 %	0.134°	0.076°

SUMMARY

Even though the jitter measurements thus far have shown that the RF system, as built, is very stable there is still room for improvements. To that effort, measurements are currently being done to determine the difference in the drive signal between the modulators at higher powers. Additional profiling is being performed on the whole RF system to determine the temperature equivalent noise power [3]. However, even with the differences, the data presented herein shows that the RF system design is well within the bounds of stated requirements and was an overall success.

REFERENCES

- [1] V. Manassewitsch, *Frequency Synthesizers: Theory and Design*, New York, NY, USA, Wiley, 1987.
- [2] S. Haykin, *Communication Systems*, New York, NY, USA, John Wiley & Sons Inc., 1978.
- [3] D. M. Pozar, *Microwave Engineering*, Hoboken, NJ, USA, Wiley, 2012.